Line Degeneracy and Strong Spin-Orbit Coupling of Light with Bulk Bianisotropic Metamaterials

Qinghua Guo,[1,2] Wenlong Gao,[1,3] Jing Chen,[2] Yongmin Liu,[4] and Shuang Zhang[1,*]
[1]School of Physics and Astronomy, University of Birmingham, Birmingham B15 2TT, United Kingdom
[2]School of Physics, Nankai University, Tianjin 300071, China
[3]State Key Laboratory of Precision Measuring Technology and Instruments, Tianjin University, Tianjin 300072, China
[4]Department of Mechanical and Industrial Engineering and Department of Electrical and Computer Engineering, Northeastern University, Boston, Massachusetts 02115, USA
(Received 26 March 2015; published 7 August 2015)

Propagation of light in a medium is dictated by equifrequency surfaces (EFSs), which play a similar role as Fermi surfaces for electrons in crystals. Engineering the equifrequency surface of light through structuring a photonic medium enables superior control over light propagation that goes beyond natural materials. In this Letter, we show that a bulk metamaterial with a suitably designed bianisotropy can exhibit line degeneracy in its EFSs that consist of two ellipsoids of opposite helicity states intersecting with each other. Very interestingly, light propagating along the direction of the line degeneracy experiences strong spin-dependent photon deflection, or optical spin Hall effect, which may lead to applications in optical signal processing and spin-optical manipulations. We provide a realistic metamaterial design to show that the required bianisotropy can be readily obtained.

DOI: 10.1103/PhysRevLett.115.067402 PACS numbers: 78.20.Ek, 42.50.Tx, 78.20.Fm, 78.67.Pt

Engineering equifrequency surfaces (EFSs) by using artificial photonic structures, such as photonic crystals and metamaterials, has generated a plethora of unconventional optical properties [1,2]. One noted example is the hyperbolic medium with a dielectric tensor consisting of elements of mixed signs; this produces unconfined EFSs that enable exceptional optical properties and applications such as negative refraction and super-resolution imaging [3–6]. In general, optical media exhibit two sheets of EFSs, corresponding to two distinct polarization states for each propagation direction. In most natural isotropic media, the two polarization states are degenerate, leading to the presence of a single degenerate spherical equifrequency surface. However, introducing anisotropy and chirality can lift the degeneracy, resulting in polarization-dependent wave propagation.

In general, the two sheets of EFSs are either completely separated, as in the case of isotropic chiral medium [7], or they touch at isolated points in the reciprocal space, as in the case of uniaxial and biaxial birefringent crystals [8]. Uniaxial birefringent crystals are the most common anisotropic medium existing in nature; their EFSs show quadratic curvatures and the two polarization states share the same tangential plane at the degeneracy points. On the other hand, the EFSs of biaxial birefringent crystals, with all three dielectric constants along the principal directions being different, exhibit degeneracy points with linear cone-shaped crossing; this gives rise to the interesting phenomenon of cone diffraction that serves as one of the most well-known examples of singular optics [9–11].

Metamaterials can be engineered to exhibit highly complex optical responses. Previously investigated properties, including negative index of refraction [12–19], hyperbolic metamaterials [20–23], and strong chirality [24–32], constitute just a small subset of the unconventional optical properties that can be achieved with metamaterials. As electromagnetic waves are vector fields, the electromagnetic parameters (permittivity, permeability, and coupling between electric and magnetic responses) of complex effective medium can be expressed by three tensors, offering a huge parameter space for controlling electromagnetic wave propagation. In this Letter, we show that with judicious engineering of the electromagnetic parameters, a novel type of metamaterials can be designed to exhibit line degeneracy between the two equifrequency ellipsoids of opposite optical spin states. For light propagating along any point in the line degeneracy, photons of different helicities are split into different directions, in analog to the spin Hall effect in electronic systems. This strong spin-orbit coupling of light can be used to design spin sorting devices with extremely high efficiency.

Within the effective medium theory, the most general form of the constitutive equations taking into account the coupling between the electric and magnetic responses is given by

$$\vec{D} = \overleftrightarrow{\varepsilon}\,\vec{E} + \overleftrightarrow{\xi}\,\vec{H}\vec{B} = \overleftrightarrow{\mu}\,\vec{H} + \overleftrightarrow{\varsigma}\,\vec{E}. \tag{1}$$

We consider that the metamaterial proposed here has the following tensors of permittivity, permeability, and bianisotropy:

$$\overleftrightarrow{\varepsilon} = \begin{pmatrix} \varepsilon_{xx} & 0 & 0 \\ 0 & \varepsilon_{yy} & 0 \\ 0 & 0 & \varepsilon_{zz} \end{pmatrix}, \quad \overleftrightarrow{\mu} = \eta^2 \overleftrightarrow{\varepsilon} = \begin{pmatrix} \mu_{xx} & 0 & 0 \\ 0 & \mu_{yy} & 0 \\ 0 & 0 & \mu_{zz} \end{pmatrix},$$
$$\overleftrightarrow{\xi} = -\overleftrightarrow{\varsigma} = \begin{pmatrix} 0 & i\gamma & 0 \\ i\gamma & 0 & 0 \\ 0 & 0 & 0 \end{pmatrix}. \tag{2}$$

As shown by Eq. (2), there exists coupling between the electric and magnetic responses along orthogonal directions, as indicated by the presence of nonzero off-diagonal elements in the coupling matrix. An additional feature of the proposed metamaterial for achieving line degeneracy is that the permittivity and permeability tensor elements are in proportion to each other. Although the coupling matrix appears different from that of chiral metamaterials, with nonzero diagonal elements to couple the electric and magnetic fields along the same direction, it will be shown later that due to the symmetry between ξ_{xy} and ξ_{yx}, the coupling matrix can be transformed into a chiral matrix consisting of only nonzero diagonal elements through a coordinate rotation.

The EFSs and the associated eigenstates of the metamaterial with above parameter tensors can be obtained by substituting the constitutive equations into Maxwell's equations. To simplify the analysis, we assume that the permittivity of the material is uniaxial and takes the form $\varepsilon_{xx} = \varepsilon_{yy} = \varepsilon_\perp$ and $\varepsilon_{zz} = \varepsilon_\parallel$. The dispersion relation can be expressed as

$$\frac{k_x^2 + k_y^2}{\varepsilon_\parallel \gamma} + \frac{2k_x k_y}{\eta \varepsilon_\perp \varepsilon_\parallel} + \frac{k_z^2}{\varepsilon_\perp \gamma} = \frac{(\varepsilon_\perp^2 \eta^2 - \gamma^2)}{\varepsilon_\perp \gamma} \omega^2$$
$$\frac{k_x^2 + k_y^2}{\varepsilon_\parallel \gamma} - \frac{2k_x k_y}{\eta \varepsilon_\perp \varepsilon_\parallel} + \frac{k_z^2}{\varepsilon_\perp \gamma} = \frac{(\varepsilon_\perp^2 \eta^2 - \gamma^2)}{\varepsilon_\perp \gamma} \omega^2. \quad (3)$$

The EFSs for a specific set of parameters $\overleftrightarrow{\varepsilon} = \mathrm{Diag}\{3, 3, 2\}$, $\eta^2 = 0.8$, and $\gamma = 1.5$ are plotted in Fig. 1, which exhibit two EFSs of ellipsoid shape. The two ellipsoids intersect with each other, forming two degeneracy lines of circular shape in the k space. These degeneracy lines exhibit optical phenomena very different from the degenerate points of conventional uniaxial and biaxial birefringent crystals. For example, in the EFSs of biaxial birefringent crystals [9–11] each degeneracy point forms a double cone. When a narrow beam is incident along the degeneracy point it will spread into a hollow cone within the crystal. On the other hand, for the bianisotropic medium studied here, due to the different directions of the group velocities of the two EFSs at the degeneracy line, a beam incident along any point on the degeneracy lines is expected to split into two separate beams of different polarization states propagating along the surface normal directions of the respective EFSs. Detailed numerical analyses show that the polarization states on the two ellipsoids are, respectively, left- and right- elliptically polarized. In Fig. 1, the colors on the EFSs represent the helicity, *i.e.,* the Stokes parameter s_3, defined by the electric displacement vector of the eigenstates, with $s_3 = 1$ and -1 denoting left-handed and right-handed circular polarization, respectively. Thus it is seen that the two states are close to circular polarization at the degeneracy lines.

The elliptically polarized eigenstates of the metamaterial can be understood by diagonalizing the coupling matrix ξ through a coordinate rotation of 45° in the xy plane, which is given by

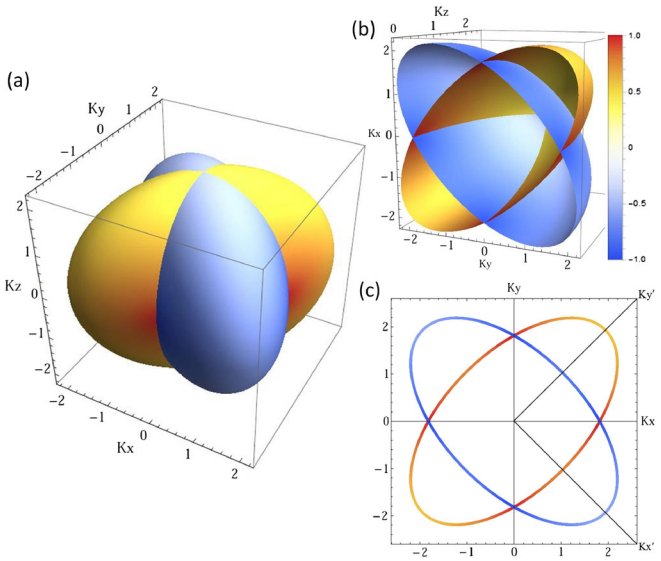

FIG. 1 (color online). Equifrequency surfaces of the bianisotropic metamaterial. (a) Two EFSs intercept each other at two degeneracy circles. (b) The cross-section view of the EFSs. (c) The 2D equifrequency contour plot at $k_z = 0$ with $\overleftrightarrow{\varepsilon} = \mathrm{Diag}\{3, 3, 2\}$, $\eta^2 = 0.8$, and $\gamma = 1.5$. The helicity (Stokes parameter s_3) is indicated by the color bar. The eigenstates of the two crossing ellipsoids EFSs are elliptically polarized with opposite handedness, as indicated by arrows.

$$\overleftrightarrow{\xi}_{\mathrm{rot}} = \begin{pmatrix} i\gamma & 0 & 0 \\ 0 & -i\gamma & 0 \\ 0 & 0 & 0 \end{pmatrix}. \quad (4)$$

Equation (4) shows that, in the new coordinate (k_x', k_y', k_z) as shown in Fig. 1(c), the coupling matrix contains nonzero diagonal elements with opposite signs, indicating that the waves propagating along the x' and y' directions exhibit opposite optical activities; this is consistent with the plot of EFSs in Fig. 1. It has been shown previously that the coupling matrix in the form of Eq. (4) can be realized with various complex 3D structures [33]. The dispersion relations of the two eigenmodes in the rotated coordinate take the simpler forms of

$$\frac{k_x'^2}{\eta \varepsilon_\parallel (\eta \varepsilon_\perp - \gamma)} + \frac{k_y'^2}{\eta \varepsilon_\parallel (\eta \varepsilon_\perp + \gamma)} + \frac{k_z^2}{\eta^2 \varepsilon_\perp^2 - \gamma^2} = \omega^2$$
$$\frac{k_x'^2}{\eta \varepsilon_\parallel (\eta \varepsilon_\perp + \gamma)} + \frac{k_y'^2}{\eta \varepsilon_\parallel (\eta \varepsilon_\perp - \gamma)} + \frac{k_z^2}{\eta^2 \varepsilon_\perp^2 - \gamma^2} = \omega^2. \quad (5)$$

Equation (5) verifies that the EFSs of the two eigenstates are ellipsoids of the same shape, but different orientations. Equation (5) also gives explicitly the lengths of the three axes of the EFS ellipsoids, which are in general different from each other.

The bianisotropic response discussed above can be implemented by a bulk metamaterial with a unit cell consisting of two intersecting split-ring resonators (SRRs)

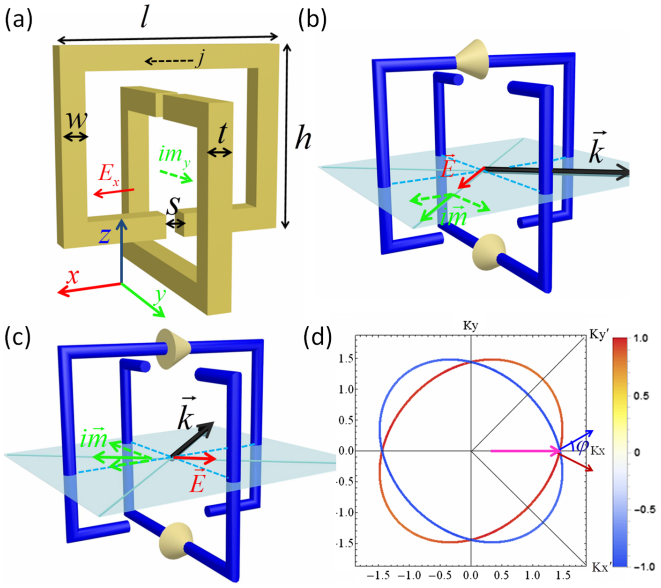

FIG. 2 (color online). Proposed unit cell of the metamaterial. (a) Schematic of the unit cell of the metamaterial. The geometrical parameters are $l = 4.8$ mm, $h = 4.0$ mm, $t = w = 0.5$ mm, and $s = 0.4$ mm. The periodicity of the unit cell is 6.0 mm in the x, y, and z direction. The bianisotropic response can be understood from the fields and current distribution for an x-polarized incidence. (b) There exists a chiral response, *i.e.,* the electric field induces a magnetic dipole along the same direction, when the incident wave propagates along the x' direction. (c) The chiral response is reversed compared to (b) when the incident wave propagates along the y' direction. (d) EFCs at $k_z = 0$ with the retrieved parameters of $\overleftrightarrow{\varepsilon} = \mathrm{Diag}\{2.22, 2.22, 1.9\}$, $\overleftrightarrow{\mu} = \mathrm{Diag}\{1.17, 1.17, 1\}$, and $\gamma = 0.37$ at 6.1 GHz.

of identical geometries lying in the xz and yz plane, respectively, which are schematically illustrated in Fig. 2(a). Each SRR is equivalent to a LC circuit, with the gap and the loop functioning as a capacitor and an inductor, respectively. The LC resonant mode simultaneously supports an electric dipole along the gap and a magnetic dipole perpendicular to the loop. For instance, the E_x component can induce a magnetic dipole along the y axis [as marked in Fig. 2(a)], while the H_y component can induce an electric dipole along the x axis. Therefore, we can achieve a bianisotropic response that couples the electric and magnetic responses along orthogonal directions [34]. In other words, each SRR corresponds to one of the off-diagonal elements in the coupling matrix $\boldsymbol{\xi}$, with the orientation of each SRR controlling the sign of the corresponding matrix element. It is shown in Fig. 2(a) that the gaps of the two SRRs are oriented in opposite directions, with one SRR facing up (the $+z$ direction) and other one facing down (the $-z$ direction). This arrangement ensures that the two off-diagonal elements ξ_{xy} and ξ_{yx} in the coupling matrix have the same sign, since a simple rotation of a SRR by 90° in the xy plane without inverting its gap orientation transforms ξ_{xy} to $-\xi_{yx}$, or transforms ξ_{yx} to $-\xi_{xy}$.

The mechanism of the direction-dependent handedness in the proposed metamaterial can be unveiled by analyzing the electromagnetic responses of the two SRRs. As shown by Fig. 2(b), for a beam propagating along the k'_x direction with TM polarization (the electric field is in the xy plane), the electric current in each SRR excited by the electric field produces a magnetic dipole moment that is perpendicular to the SRR (dashed green arrows). The overall magnetic dipole moment (the solid green arrow), being the sum of dipole moments from both SRRs, is along the same direction as that of the incident electric field. The collinearity of the electric field and the generated magnetic dipole moment indicates the presence of handedness, *i.e.*, optical activities. On the other hand, for a beam propagating along the k'_y direction with TM polarization, the induced overall magnetic dipole moment is opposite to the direction of the electric field, leading to an inversion of the handedness relative to the propagation along the k'_x direction. Therefore, the metamaterial behaves as an effective medium with k-dependent handedness [33], in which the sign of the optical activity can be flipped for light propagating along two orthogonal directions. It should be noted that twisted SRRs have been used to generate a bianisotropic electromagnetic response previously [35,36]. However, the magnetic dipole moments of the two SRRs in those works are along the same direction, and, therefore, they do not generate the direction-dependent handedness as presented here.

The EFSs of the metamaterial with geometry specified in Fig. 2(a) are obtained by using the eigenmode solver of the commercial software CST MICROWAVE STUDIO™ (Supplemental Material [37]). The effective parameters of the metamaterial are subsequently retrieved from the numerically obtained EFSs (details of retrieval are given in the Supplemental Material [37]). The retrieval results are $\overleftrightarrow{\varepsilon} = \mathrm{Diag}\{2.22, 2.22, 1.9\}$, $\overleftrightarrow{\mu} = \mathrm{Diag}\{1.17, 1.17, 1\}$, and $\gamma = 0.37$ at 6.1 GHz, which fulfill the requirements of proportionality between the permittivity and permeability tensors for the existence of the degeneracy line. Note that the operation frequency is far from the resonance frequency to avoid strong dispersion and loss of the effective electromagnetic parameters. The EFSs are calculated and their cross sections at $k_z = 0$ are shown in Fig. 2(d), which confirm that the two EFSs are degenerate along the k_x and k_y directions. Though the two eigenpolarization states share the same wave vector at the degeneracy line, they exhibit helicity-dependent group velocities because of the linear crossing. Full-wave simulations by using these extracted effective parameters verify the spin-dependent beam deflection for beam incidence along the degeneracy point. As the eigenstates of the electric field on the two ellipses are left- and right-elliptically polarized, it is expected that the excitation of each mode is dependent on the helicity of the incident beam. As shown in Fig. 3(a), when the incident beam is linearly polarized, both photonic modes on the two EFSs are equally excited, and they propagate in the direction along the normal of their respective EFSs. The deflection angle can be determined by the normal direction

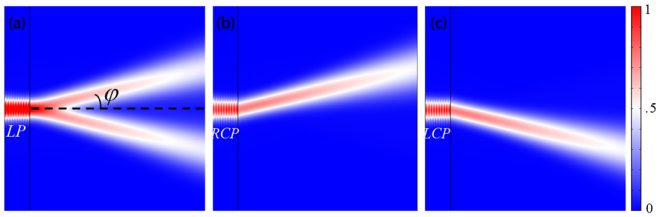

FIG. 3 (color online). Simulated field distribution for (a) linearly, (b) right-handed circularly, and (c) left-handed circularly polarized incidence in the xy plane. The wave is incident along the x direction from vacuum to the metamaterial, and the parameters of the metamaterial are retrieved from the coupled SRR structure.

of the two ellipses at the crossing point. For the electromagnetic wave incident along the x direction, the deflected angle of the propagating mode can be calculated as $\varphi = \arctan(\gamma/\eta\varepsilon_{xx})$, which is 12.94° for the parameters of the metamaterial investigated here. In the simulation, when the incident beam is circularly polarized, it is primarily refracted into a single direction, as shown in Fig. 3(b). Reversing the circular polarization of the incident beam leads to the flipping of the propagation direction to the other side of the surface normal [Fig. 3(c)].

Next we derive the transmission coefficients for different polarizations of the incident light (see Supplemental Material [37] for details). When the incident wave is right-circularly polarized, the excitation relative ratio of the left- and right-polarized modes is given by

$$\delta = t_{-+}/t_{++} = \frac{|(\eta-1)(1-\eta a)|}{\eta(1+a)+(1+\eta^2 a)} \quad \text{with} \quad a = \sqrt{\frac{\varepsilon_{xx}\varepsilon_{zz}}{-\gamma^2+\varepsilon_{xx}\varepsilon_{yy}\eta^2}}. \tag{6}$$

By using the retrieved effective parameters of the metamaterial at 6.1 GHz, we obtain a very small ratio between the cross and the cocircular polarization transmission $\delta \approx 0.004$, indicating that a circularly polarized incident light only couples to the propagating mode of the same helicity. This is consistent with the simulated field shown in Fig. 3.

In the preceding analysis we have chosen a frequency where the permittivity and permeability tensors are proportional to each other for achieving the degeneracy lines. However, the proportionality can only be obtained at a particular frequency. Away from this frequency, proportionality is in general not satisfied, because permittivity and permeability have different dispersion relations. For instance, at a frequency of 6.8 GHz the retrieval effective parameters of the same metamaterial are $\overleftrightarrow{\varepsilon} = \mathrm{Diag}\{2.663, 2.663, 2.186\}$, $\overleftrightarrow{\mu} = \mathrm{Diag}\{1.19, 1.19, 1\}$, and $\gamma = 0.559$. The permittivity and permeability slightly deviate from the proportionality condition, with $\varepsilon_{xx(yy)}/\mu_{xx(yy)} = 2.238$ and $\varepsilon_{zz}/\mu_{zz} = 2.186$. The EFSs at this frequency are calculated and shown in Fig. 4(a). It is observed that the degeneracy is broken, and a small gap appears with a width given by

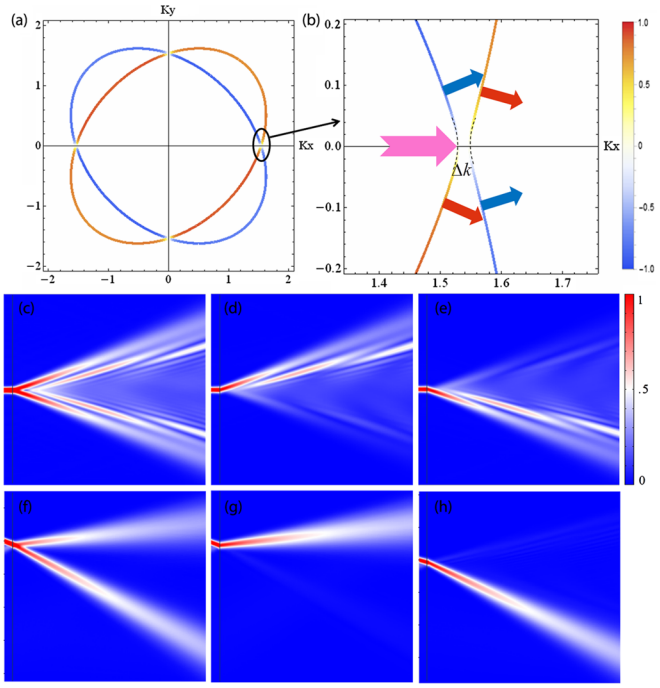

FIG. 4 (color online). Wave propagation inside a metamaterial with permittivity and permeability tensors slightly out of proportion. (a) Nondegenerate EFCs for the retrieved effective parameters at a frequency of 6.8 GHz. (b) Enlarged view of the gap between the two EFCs. The arrows showing the group velocity direction of the modes, with red and blue colors representing left-handed and right-handed elliptical polarization, respectively. Simulated field magnitude in the effective medium for a (c) linearly, (d) right-handed circularly, and (e) left-handed circularly polarized incident beam at normal incidence. (f)–(h) are similar to (c)–(e) but for oblique incidence with incident angle 20°.

$$\Delta k = \left(\sqrt{\mu_\parallel/\mu_\perp} - \sqrt{\varepsilon_\parallel/\varepsilon_\perp}\right)\sqrt{(\varepsilon_\perp\mu_\perp - \gamma^2)} \tag{7}$$

The lift of degeneracy converts the linear crossing of the two EFCs into two separated quadratic curves, and, consequently, the beam diverges inside the metamaterial due to the broad range of group velocities, as illustrated by Figs. 4(a) and 4(b). Interestingly, interference fringes are observed in the field pattern, as shown in Figs. 4(c)–4(e). The fringes are due to the beating of the different wave vectors with the same group velocity and helicity, corresponding to the curve sections with the same color as shown in Fig. 4(b). Despite the lift of degeneracy, the helicity-selective routing of light still persists, because the circularly polarized incident light is primarily refracted into one side of the surface normal, and can be switched to the other side by reversing the helicity of the incident beam. These results are shown in Figs. 4(d) and 4(e). Note that interference pattern usually occurs when there are multiple beams propagating along different directions. The observed interference pattern in the metamaterial arises solely from the interference between different wave vector components

within a single beam. This new phenomenon has not been observed previously in homogenous effective media.

The fringe patterns can be eliminated by setting the incident Gaussian beam to an oblique angle of 20°, as shown in Fig. 4(f). Because of the oblique incidence, light is coupled primarily to the propagation modes on one side of the surface normal; therefore, the interference between the wave components with the same group velocity and helicity but residing on different quadratic equifrequency curves is minimized. It is observed that the propagation of beam inside the metamaterial is almost identical to the case with line degeneracy [Figs. 3(b)–3(c)]; *i.e.,* the propagation direction of the beam can be almost completely switched to the other side by reversing the helicity of the incident beam, as shown in Figs. 4(g) and 4(h).

In conclusion, we have proposed and theoretically investigated a new type of metamaterials that exhibit line degeneracy in their EFSs, accompanied by a strong spin-orbit coupling of light. Although we have demonstrated the metamaterials at the GHz regime, we would like to point out that the structure can in principle be extended to infrared frequencies, where strong magnetic response and bianisotropy have been realized previously using the SRR design [38,39]. Because of the scaling effect, further extension to visible range leads to very weak magnetic responses. However, it is envisaged that dielectric material with large permittivity could be a possible candidate for realizing a strong bianisotropy effect at visible and near-infrared frequencies. Our research findings may provide a route for various applications involving the spin degree of freedom of light, such as quantum information processing and chemical sensing.

This work was supported by Leverhulme Trust (Grant No. RPG-2012-674) and National Science Foundation of China (Grant No. 61328503 and No. 11174157)

*s.zhang@bham.ac.uk

[1] N. Masaya, Manipulating light with strongly modulated photonic crystals, Rep. Prog. Phys. **73**, 096501 (2010).
[2] C. M. Soukoulis and M. Wegener, Past achievements and future challenges in the development of three-dimensional photonic metamaterials, Nat. Photonics **5**, 523 (2011).
[3] Y. Liu, G. Bartal, and X. Zhang, All-angle negative refraction and imaging in a bulk medium made of metallic nanowires in the visible region, Opt. Express **16**, 15439 (2008).
[4] X. Zhang and Z. Liu, Superlenses to overcome the diffraction limit, Nat. Mater. **7**, 435 (2008).
[5] A. Poddubny, I. Iorsh, P. Belov, and Y. Kivshar, Hyperbolic metamaterials, Nat. Photonics **7**, 948 (2013).
[6] L. Ferrari, C. Wu, D. Lepage, X. Zhang, and Z. Liu, Hyperbolic metamaterials and their applications, Prog. Quantum Electron. **40**, 1 (2015).
[7] W. Gao, M. Lawrence, B. Yang, F. Liu, F. Fang, B. Béri, J. Li, and S. Zhang, Topological Photonic Phase in Chiral Hyperbolic Metamaterials, Phys. Rev. Lett. **114**, 037402 (2015).
[8] A. Yariv, *Optical Waves in Crystals: Propagation and Control of Laser Radiation* (Wiley-Interscience, New York, 2002).
[9] M. V. Berry, Conical diffraction asymptotics: Fine structure of Poggendorff rings and axial spike, J. Opt. A **6**, 289 (2004).
[10] M. V. Berry, M. R. Jeffrey, and J. G. Lunney, Conical diffraction: Observations and theory, Proc. R. Soc. A **462**, 1629 (2006).
[11] M. V. Berry and M. R. Jeffrey, Conical diffraction: Hamilton's diabolical point at the heart of crystal optics, in *Progress in Optics* (Elsevier, Amsterdam, 2007), Vol. 50, pp. 13–50.
[12] J. B. Pendry, Negative Refraction Makes a Perfect Lens, Phys. Rev. Lett. **85**, 3966 (2000).
[13] R. A. Shelby, D. R. Smith, and S. Schultz, Experimental verification of a negative index of refraction, Science **292**, 77 (2001).
[14] D. R. Smith, J. B. Pendry, and M. C. K. Wiltshire, Metamaterials and negative refractive index, Science **305**, 788 (2004).
[15] V. M. Shalaev, W. S. Cai, U. K. Chettiar, H. K. Yuan, A. K. Sarychev, V. P. Drachev, and A. V. Kildishev, Negative index of refraction in optical metamaterials, Opt. Lett. **30**, 3356 (2005).
[16] S. Zhang, W. J. Fan, N. C. Panoiu, K. J. Malloy, R. M. Osgood, and S. R. J. Brueck, Experimental Demonstration of Near-Infrared Negative-Index Metamaterials, Phys. Rev. Lett. **95**, 137404 (2005).
[17] C. M. Soukoulis, S. Linden, and M. Wegener, Negative refractive index at optical wavelengths, Science **315**, 47 (2007).
[18] V. M. Shalaev, Optical negative-index metamaterials, Nat. Photonics **1**, 41 (2007).
[19] S. Zhang, Y.-S. Park, J. Li, X. Lu, W. Zhang, and X. Zhang, Negative Refractive Index in Chiral Metamaterials, Phys. Rev. Lett. **102**, 023901 (2009).
[20] Z. Jacob, L. V. Alekseyev, and E. Narimanov, Optical hyperlens: Far-field imaging beyond the diffraction limit, Opt. Express **14**, 8247 (2006).
[21] A. Salandrino and N. Engheta, Far-field subdiffraction optical microscopy using metamaterial crystals: Theory and simulations, Phys. Rev. B **74**, 075103 (2006).
[22] Z. Liu, H. Lee, Y. Xiong, C. Sun, and X. Zhang, Far-field optical hyperlens magnifying sub-diffraction-limited objects, Science **315**, 1686 (2007).
[23] J. Yao, Z. Liu, Y. Liu, Y. Wang, C. Sun, G. Bartal, A. M. Stacy, and X. Zhang, Optical negative refraction in bulk metamaterials of nanowires, Science **321**, 930 (2008).
[24] A. Papakostas, A. Potts, D. M. Bagnall, S. L. Prosvirnin, H. J. Coles, and N. I. Zheludev, Optical Manifestations of Planar Chirality, Phys. Rev. Lett. **90**, 107404 (2003).
[25] V. A. Fedotov, P. L. Mladyonov, S. L. Prosvirnin, A. V. Rogacheva, Y. Chen, and N. I. Zheludev, Asymmetric Propagation of Electromagnetic Waves through a Planar Chiral Structure, Phys. Rev. Lett. **97**, 167401 (2006).
[26] A. V. Rogacheva, V. A. Fedotov, A. S. Schwanecke, and N. I. Zheludev, Giant Gyrotropy due to Electromagnetic-Field Coupling in a Bilayered Chiral Structure, Phys. Rev. Lett. **97**, 177401 (2006).
[27] V. A. Fedotov, A. S. Schwanecke, N. I. Zheludev, V. V. Khardikov, and S. L. Prosvirnin, Asymmetric transmission of light and enantiomerically sensitive plasmon

resonance in planar chiral nanostructures, Nano Lett. **7**, 1996 (2007).

[28] M. Kuwata-Gonokami, N. Saito, Y. Ino, M. Kauranen, K. Jefimovs, T. Vallius, J. Turunen, and Y. Svirko, Giant Optical Activity in Quasi-Two-Dimensional Planar Nanostructures, Phys. Rev. Lett. **95**, 227401 (2005).

[29] B. Wang, J. Zhou, T. Koschny, M. Kafesaki, and C. M. Soukoulis, Chiral metamaterials: Simulations and experiments, J. Opt. A **11**, 114003 (2009).

[30] J. K. Gansel, M. Thiel, M. S. Rill, M. Decker, K. Bade, V. Saile, G. von Freymann, S. Linden, and M. Wegener, Gold helix photonic metamaterial as broadband circular polarizer, Science **325**, 1513 (2009).

[31] M. D. Turner, M. Saba, Q. Zhang, B. P. Cumming, G. E. Schröder-Turk, and M. Gu, Miniature chiral beamsplitter based on gyroid photonic crystals, Nat. Photonics **7**, 801 (2013).

[32] K. Hannam, D. A. Powell, I. V. Shadrivov, and Y. S. Kivshar, Broadband chiral metamaterials with large optical activity, Phys. Rev. B **89**, 125105 (2014).

[33] E. Efrati and W. T. M. Irvine, Orientation-Dependent Handedness and Chiral Design, Phys. Rev. X **4**, 011003 (2014).

[34] J. A. Reyes-Avendaño, U. Algredo-Badillo, P. Halevi, and F. Pérez-Rodríguez, From photonic crystals to metamaterials: The bianisotropic response, New J. Phys. **13**, 073041 (2011).

[35] H. Liu, D. A. Genov, D. M. Wu, Y. M. Liu, Z. W. Liu, C. Sun, S. N. Zhu, and X. Zhang, Magnetic plasmon hybridization and optical activity at optical frequencies in metallic nanostructures, Phys. Rev. B **76**, 073101 (2007).

[36] T. Q. Li, H. Liu, T. Li, S. M. Wang, F. M. Wang, R. X. Wu, P. Chen, S. N. Zhu, and X. Zhang, Magnetic resonance hybridization and optical activity of microwaves in a chiral metamaterial, Appl. Phys. Lett. **92**, 131111 (2008).

[37] See Supplemental Material at http://link.aps.org/supplemental/10.1103/PhysRevLett.115.067402 for the retrieval of the effective parameters of the metamaterial and the transmission coefficients for different polarization states of the incident light.

[38] W. J. Padilla, D. R. Smith, and D. N. Basov, Spectroscopy of metamaterials from infrared to optical frequencies, J. Opt. Soc. Am. B **23**, 404 (2006).

[39] X. Xu, B. Quan, C. Gu, and L. Wang, Bianisotropic response of microfabricated metamaterials in the terahertz region, J. Opt. Soc. Am. B **23**, 1174 (2006).